

Propagation front of correlations in an interacting Bose gas

Peter Barmettler¹, Dario Poletti¹, Marc Cheneau², and Corinna Kollath^{1,3}

¹*Département de Physique Théorique, Université de Genève, 1211 Genève, Switzerland*

²*Max-Planck-Institut für Quantenoptik, 85748 Garching, Germany and*

³*Centre de physique théorique, École Polytechnique, CNRS, 91128 Palaiseau, France*

(Dated: Thu 27th Sept, 2018)

We analyze the quench dynamics of a one-dimensional bosonic Mott insulator and focus on the time evolution of density correlations. For these we identify a pronounced propagation front, the velocity of which, once correctly extrapolated at large distances, can serve as a quantitative characteristic of the many-body Hamiltonian. In particular, the velocity allows the weakly interacting regime, which is qualitatively well described by free bosons, to be distinguished from the strongly interacting one, in which pairs of distinct quasiparticles dominate the dynamics. In order to describe the latter case analytically, we introduce a general approximation to solve the Bose–Hubbard Hamiltonian based on the Jordan–Wigner fermionization of auxiliary particles. This approach can also be used to determine the ground-state properties. As a complement to the fermionization approach, we derive explicitly the time-dependent many-body state in the non-interacting limit and compare our results to numerical simulations in the whole range of interactions of the Bose–Hubbard model.

I. INTRODUCTION

In the past two decades, progress in atomic physics, quantum optics, and the nanosciences has propelled quantum many-body theory to meet new challenges. It is indeed now possible to engineer systems that are concrete realizations of some paradigmatic models, which were once introduced to grasp fundamental properties of more complex materials. New frontiers thus have to be explored, among which the dynamics of these isolated quantum models far from equilibrium is probably the least well understood and one of the most exciting.

One of the fundamental questions that has to be addressed is how correlations propagate in these systems. The Schrödinger equation allows in principle for correlations between distant points to build up in arbitrary short times [1]. This contrasts with relativistic quantum field theories, where physical effects cannot propagate faster than the speed of light and causality relations between two points in space-time can exist only if one lies within the light-cone of the other. In a seminal work [2], Lieb and Robinson however showed that non-relativistic quantum many-body systems can still exhibit some sort of locality: In generic one-dimensional spin models with finite-range interactions, the propagation of correlations appears to be bounded by an effective light cone, outside which correlations are exponentially suppressed. Here the role of the speed of light is played by a velocity which is an intrinsic property of the many-body Hamiltonian. The existence of so-called Lieb–Robinson bounds has many far-reaching implications. For example, they make it possible to simulate on classical computers the ground state properties as well as the dynamical evolution of such quantum systems [3–6]. They also provide a general link between the presence of a finite spectral gap and the existence of a finite correlation length in the ground state of certain lattice systems [7–10]. However, the extent to which Lieb–Robinson bounds can be generalized beyond spin systems remains an open ques-

tion. Proofs or evidence for the existence of such bounds have indeed been reported in various systems, ranging from harmonic chains to the Bose–Hubbard model [11–16]. But it is also possible to construct models in which the propagation velocity of correlations is explicitly unbounded [17].

Dynamical properties of correlations in a closed system can be probed by studying the time evolution following a sudden change of parameter in the Hamiltonian, a situation referred to as a *quantum quench*. The quench has a particular appeal in the context of ultracold gases in optical lattices as the relevant parameters in the Hamiltonian governing these systems can be easily varied in time [18]. In addition to the existence of an effective light cone, it was discovered in recent theoretical studies that the time evolution of correlations in quenched systems is characterized by a pronounced propagation front [11, 12, 15, 16, 19–26]. As for a Lieb–Robinson bound, the velocity at which this front propagates can involve a broad range of the spectrum of the Hamiltonian since the system is far from equilibrium. This makes the understanding of this feature particularly challenging: Covariant low-energy effective theories would provide a natural description [11, 12, 20–22], but, due to the presence of high-energy excitations, realistic lattice models [11, 12, 15, 16, 19, 23–33] show a much richer behavior than their corresponding field theories. Gaining more insight into the non-equilibrium properties of quantum systems thus urges the development of new effective models.

In a recent work [19], the propagation of correlations in a quantum many-body system was studied both theoretically and experimentally in a one-dimensional bosonic gas in an optical lattice and a propagation front could be clearly identified. The observed behavior was interpreted using an exactly solvable effective model derived from the Bose–Hubbard Hamiltonian and describing non-interacting fermionic quasiparticles. The key idea behind this model is to use a Jordan–Wigner transformation to

cure some of the problems inherent to the slave-boson methods proposed previously [34, 35]. In the present article, we describe this approach in more detail and use it to derive the ground state as well as the quench dynamics in the Mott-insulating phase. We show that its predictions are quantitatively correct in a regime of strong and intermediate interactions. Our model, being exactly solvable, allows us to explore the time evolution of the system at long times, and we can show that the velocity of the propagation front exhibits a generic scaling behavior. Using numerical simulations, we find that this behavior holds in all interaction regimes, down to the non-interacting limit of free bosons, where explicit solutions are available. The asymptotic value of the velocity of the propagation front, which strongly differs between the strongly and the weakly interacting limits, can be used to characterize the crossover between these two regimes.

This article is organized as follows: In Sec. II we present the model that we will study; in Sec. III we carry out the fermionization procedure and derive general relations that enable the calculation of equilibrium (Sec. IV) and non-equilibrium (Sec. V) properties. The velocity of the propagation front at weak and strong interactions is analyzed in Sec. VI. In Sec. VII we present our conclusions.

II. ONE-DIMENSIONAL SYSTEM OF BOSONIC ATOMS IN AN OPTICAL LATTICE

In this work we consider a one-dimensional system of bosonic atoms in an optical lattice. If the lattice is deep enough, this system can be described by the one-dimensional single-band Bose–Hubbard Hamiltonian:

$$H = \sum_j \left\{ -J (a_j^\dagger a_{j+1} + \text{h. c.}) + \frac{U}{2} (n_j - \bar{n})^2 \right\}, \quad (1)$$

where a_j and a_j^\dagger represent the annihilation and creation operators of a bosonic atom at site j and $n_j = a_j^\dagger a_j$ counts the number of atoms at that site. We use a lattice constant $a_{\text{lat}} = 1$ and the system is considered to be infinitely large and homogeneous. The kinetic part of the Hamiltonian is characterized by the hopping amplitude J ; the on-site interaction strength U is related to the s -wave scattering length. We work at fixed commensurate filling \bar{n} , where the model exhibits a quantum phase transition between a superfluid phase at low interaction strengths $U/J < (U/J)_c$ and a Mott-insulating phase at large interaction strengths $U/J > (U/J)_c$. At the specific filling $\bar{n} = 1$, the critical value is given by $(U/J)_c \sim 3.4$ [36, 37]. The Bose–Hubbard model is non-integrable [38, 39] and exhibits complex many-body properties; in particular, its non-equilibrium properties are far from being fully understood.

In order to benchmark the analytical approaches, we will perform exact numerical simulations of model (1) by means of the density matrix renormalization group

(DMRG) [40, 41], an algorithm based on matrix product states [5]. While the DMRG algorithm gives highly accurate results for the ground state, time evolution [42–44] can be calculated only for relatively short periods of time.

III. FERMIONIZATION APPROACH TO THE STUDY OF THE BOSE–HUBBARD MODEL

In the following, we will describe in detail how the Bose–Hubbard model can be mapped onto an effective model of non-interacting auxiliary fermions. The procedure consists of four main steps: (i) The local Hilbert space is reduced to only three states and (ii) auxiliary bosonic operators are introduced that allow switching between these states (Sec. III A); (iii) the auxiliary boson operators are fermionized by a Jordan-Wigner transformation (Sec. III B); (iv) a constraint on the fermionic operators is relaxed so that the effective Hamiltonian becomes quadratic and can be diagonalized (Sec. III C).

A. Auxiliary boson representation

In the Mott-insulating phase and away from the critical point, the local density fluctuations around the average filling \bar{n} are limited. It is thus possible to truncate the local basis on a single site j to three states only: $|\bar{n} + m\rangle_j$, with $m = -1, 0, 1$. Within this reduced basis, one can represent the bare atomic operators $a_j^{(\dagger)}$ in terms of constrained auxiliary boson operators $b_{j,\sigma}^{(\dagger)}$ with two flavors $\sigma = \pm 1 \equiv \pm$:

$$a_j^\dagger = \sqrt{\bar{n} + 1} b_{j,+}^\dagger + \sqrt{\bar{n}} b_{j,-}. \quad (2)$$

The ‘+’-bosons correspond to excess particles: $b_{j,+}^\dagger |\bar{n}\rangle_j = |\bar{n} + 1\rangle_j$, and ‘-’-bosons to holes: $b_{j,-}^\dagger |\bar{n}\rangle_j = |\bar{n} - 1\rangle_j$. The local Fock state $|\bar{n}\rangle_j$ represents the vacuum state of the auxiliary particles $b_{j,\sigma} |\bar{n}\rangle_j = 0$. Bosonic commutation relations are obeyed:

$$\begin{aligned} [b_{j,\sigma}, b_{j',\sigma'}^\dagger] &= \delta_{j,j'} \delta_{\sigma,\sigma'}, \\ [b_{j,\sigma}^\dagger, b_{j',\sigma'}^\dagger] &= [b_{j,\sigma}, b_{j',\sigma'}] = 0, \end{aligned} \quad (3)$$

which allow for the unphysical situation of single sites being occupied by more than one auxiliary boson. Therefore, the auxiliary operators have to fulfill the hardcore constraint

$$\left(b_{j,\sigma}^\dagger \right)^2 = (b_{j,\sigma})^2 = 0 \quad (4)$$

and double occupancies of different species need to be eliminated by imposing

$$b_{j,+}^\dagger b_{j,+} + b_{j,-}^\dagger b_{j,-} = 0. \quad (5)$$

This representation in terms of doubly-flavored constrained bosons is slightly different from the one used in slave-particle techniques [34, 35, 45–48], in which one introduces one auxiliary operator for each of the three local states $|\bar{n} + m\rangle_j$ and the number of auxiliary bosons per site is constrained to be exactly one.

B. Fermionization

It is difficult to ensure the operator constraints (4) and (5) in general, and one often resorts to mean-field [46–48] and perturbative [34, 35, 48] approximations. In the special one-dimensional case, however, it is possible to use Jordan–Wigner transformations [49, 50] which allow on the one hand for the exact treatment of the hard-core constraint (4) and on the other for suppression of local pairing of auxiliary particles.

Here, we follow the standard procedure of Jordan and Wigner [49] and introduce auxiliary fermion operators $c_{j,\sigma}$ with number operators $n_{j,\sigma} = c_{j,\sigma}^\dagger c_{j,\sigma}$ and anti-commutation relations

$$\begin{aligned} \{c_{j,\sigma}, c_{j',\sigma'}^\dagger\} &= \delta_{j,j'} \delta_{\sigma,\sigma'}, \\ \{c_{j,\sigma}^\dagger, c_{j',\sigma'}^\dagger\} &= \{c_{j,\sigma}, c_{j',\sigma'}\} = 0. \end{aligned} \quad (6)$$

Using non-local string operators,

$$\begin{aligned} Z_{j,+} &= e^{i\pi \sum_{\sigma,j' < j} n_{j',\sigma}}, \\ Z_{j,-} &= Z_{j,+} e^{i\pi n_{j,+}}, \end{aligned} \quad (7)$$

we relate the auxiliary bosonic operators to the fermionic ones:

$$b_{j,\sigma} = Z_{j,\sigma} c_{j,\sigma}. \quad (8)$$

The string operator $Z_{j,\sigma}$ counts the parity of the number of fermions accumulated over all sites $j' < j$ (including the $+$ -fermion on site j if $\sigma = -$) and obeys the relations

$$Z_{j,\sigma}^\dagger = Z_{j,\sigma}, \quad Z_{j,\sigma}^2 = 1. \quad (9)$$

As a consequence, the number operators within both fermionic and bosonic representations coincide:

$$b_{j,\sigma}^\dagger b_{j,\sigma} = c_{j,\sigma}^\dagger c_{j,\sigma}, \quad (10)$$

and the original atom number operator can be written as

$$n_j = n_{j,+} - n_{j,-} + \bar{n}. \quad (11)$$

Due to the fermionic statistics, the hard-core conditions (4) are satisfied automatically. The remaining constraint (5) can be formally accounted for by the global projector $\mathcal{P} = \prod_j \mathcal{P}_j$, with $\mathcal{P}_j = (1 - n_{j,+} n_{j,-})$ eliminating states with both species on the same site. It is now possible to show that, within the truncated Hilbert space,

the original Hamiltonian (1) can be exactly represented by the following fermionic model:

$$\begin{aligned} H = \sum_j \mathcal{P} \left\{ -J(\bar{n} + 1) c_{j,+}^\dagger c_{j+1,+} - J\bar{n} c_{j+1,-}^\dagger c_{j,-} \right. \\ \left. - J\sqrt{\bar{n}(\bar{n} + 1)} \left(c_{j,+}^\dagger c_{j+1,-}^\dagger - c_{j,-} c_{j+1,+} \right) + \text{h.c.} \right. \\ \left. + \frac{U}{2} (n_{j,+} + n_{j,-}) \right\} \mathcal{P}. \quad (12) \end{aligned}$$

We note that the effective hopping amplitudes for the two different flavors differ by the bosonic enhancement factor of Eq. (2).

C. Exact diagonalization within the approximation of unconstrained fermions

In practice, it is difficult to take care analytically of the projector \mathcal{P} . We will thus carry out the calculations in the approximation of unconstrained fermions (UF), $\mathcal{P} \rightarrow 1$, leading to a quadratic Hamiltonian that can be diagonalized exactly. We will see that the UF approximation is justified because the main source of creation of double occupancies would be a local pairing mechanism, which, in the fermionic representation, is suppressed by the statistics of the auxiliary particles.

The Hamiltonian (12) with $\mathcal{P} \equiv 1$ can be rewritten in momentum space as

$$\begin{aligned} H_{\text{UF}} = \sum_{\sigma,k} E_\sigma(k) c_{k,\sigma}^\dagger c_{k,\sigma} \\ + \sum_k \Delta(k) (c_{k,+}^\dagger c_{-k,-}^\dagger - c_{-k,-} c_{k,+}), \end{aligned} \quad (13)$$

with the bare dispersions

$$E_+(k) = -2J(\bar{n} + 1) \cos(k) + U/2, \quad (14a)$$

$$E_-(k) = -2J\bar{n} \cos(k) + U/2, \quad (14b)$$

and an antisymmetric pairing parameter

$$\Delta(k) = i2J\sqrt{\bar{n}(\bar{n} + 1)} \sin(k), \quad (15)$$

which obeys $\Delta(-k) = -\Delta(k) = \Delta^*(k)$. In analogy to the Gutzwiller approximation [51–53], the accuracy of the UF approximation can be estimated *via* the translation-invariant expectation value of the local projector

$$p_{+-} = 1 - \langle \mathcal{P}_j^2(t) \rangle = \langle n_{j,+} n_{j,-} \rangle. \quad (16)$$

This quantity is a measure for the population of unphysical states and gives the order of magnitude of the error in local observables (due to translational invariance site indices of observables can be dropped). Additionally, we will study the quality of the relaxation of the constraint (5) by comparison to the numerically exact DMRG method.

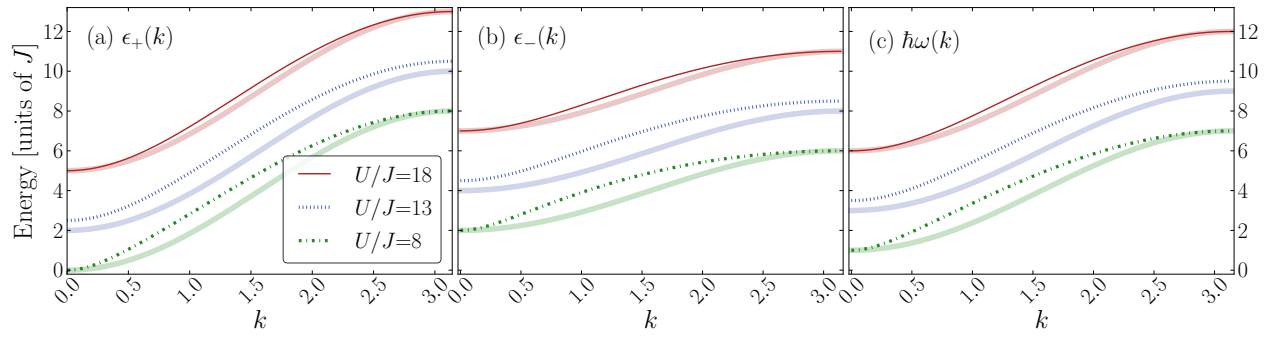


FIG. 1. (Color online) Quasiparticle dispersions (Eq. 21 and Eq. 22a) at $\bar{n} = 1$ for different interaction strengths (thin lines). Curvatures can deviate significantly from the cosine form of the strong coupling limit (thick lines). The width and the gap of the quasiparticle bands depend on the type of quasiparticle. At $U/J = 8$, the gap of the $+$ -particle closes, signaling the breakdown of the UF approximation.

The quadratic Hamiltonian H_{UF} can be diagonalized via a Bogolyubov transformation by introducing the quasiparticle operators

$$\gamma_{k,+}^\dagger = u(k)c_{k,+}^\dagger + v(k)c_{-k,-}, \quad (17a)$$

$$\gamma_{k,-}^\dagger = u(k)c_{k,-}^\dagger - v(k)c_{-k,+}. \quad (17b)$$

The functions $u(k)$ and $v(k)$ fulfill the relations

$$u(-k) = u(k) = u^*(-k), \quad (18a)$$

$$v(-k) = -v(k) = v^*(k), \quad (18b)$$

and are determined by the following expressions:

$$u(k) = \cos \left(\text{atan} \left(\frac{-2i\Delta(k)}{E_+(k) + E_-(k)} \right) / 2 \right) \quad (19a)$$

$$= 1 + \mathcal{O} \left(\frac{J^2}{U^2} \right), \quad (19b)$$

$$v(k) = i \sin \left(\text{atan} \left(\frac{-2i\Delta(k)}{E_+(k) + E_-(k)} \right) / 2 \right) \quad (19c)$$

$$= i \frac{2J\sqrt{\bar{n}(\bar{n}+1)}}{U} \sin(k) + \mathcal{O} \left(\frac{J^3}{U^3} \right). \quad (19d)$$

We infer from the above equations that the $+$ -modes are excess particles each dressed with absent holes and the $-$ -modes are holes dressed with absent excess particles. This is particularly evident from the perturbative expressions (19b) and (19d). We also note that the quasiparticle operators (17) can be interpreted as Dirac spinors [54].

Using the quasiparticle operators, the Hamiltonian can be written in the diagonal form

$$H_{\text{UF}} = \sum_{k,\sigma} \epsilon_\sigma(k) \gamma_{k,\sigma}^\dagger \gamma_{k,\sigma}. \quad (20)$$

The dispersion relation of the individual quasiparticles is

$$\epsilon_\sigma(k) = -\sigma J \cos(k) + \hbar\omega(k). \quad (21)$$

Here $2\hbar\omega(k)$ is the energy of a pair of two distinct types of quasiparticles with opposite momenta, which is given by

$$2\hbar\omega(k) = \sqrt{[E_+(k) + E_-(k)]^2 + 4|\Delta(k)|^2} \quad (22a)$$

$$= U - 2J(2\bar{n} + 1) \cos(k) + \mathcal{O} \left(\frac{J^2}{U} \right). \quad (22b)$$

The exact dispersion relations for different interaction strengths are displayed in Fig. 1, together with the first order expansion in J/U (strong coupling expansion). One can see that the profiles rapidly differ from their limiting cosine shape as the interactions are lowered. Eqs. (14) and (22a) show that the width of the energy bands depends only on the hopping amplitude J and on the average filling \bar{n} (via the Bose enhancement factor), but does not depend on the interaction strength. At large interaction strengths, the energy gap is proportional to the interaction strength and the gap of the $+$ -quasiparticles is strictly positive when the interaction is above a certain threshold:

$$U/J > 4(\bar{n} + 1). \quad (23)$$

Below this threshold our UF approximation breaks down. For $\bar{n} = 1$, the range of validity of our model is thus limited to $U/J > 8$, which is above the superfluid to Mott-insulator transition $(U/J)_c \approx 3.4$, but significantly lower than the mean-field transition $(U/J)_c \approx 12$. A description of the phase transition might be achieved by introducing auxiliary operators on the basis of a coherent-state representation (see e.g. [35]), but this goes beyond the scope of this work.

The slope of the dispersion relations $\epsilon_\sigma(k)$ describes the group velocity of the quasiparticles. Of particular interest will be the relative velocity of pairs of quasiparticles of distinct types and opposite momenta:

$$v(k) = 2 \frac{d}{dk} \omega(k), \quad (24)$$

whose maximal value

$$v_{\max} = \max_k |v(k)| \quad (25)$$

plays an important role in the characterization of the non-equilibrium properties. This maximal velocity corresponds to the point where the curvature of $\omega(k)$ changes sign. It is located at $|k| \approx \pi/2$ at large interaction strengths and is shifted toward lower momenta at smaller interaction strengths, as can be seen in Fig 1. In the relevant interaction regime (23), the maximum velocity is well approximated by:

$$v_{\max} \approx \frac{2J(2\bar{n}+1)}{\hbar} \left(1 - \frac{8\bar{n}(\bar{n}+1)J^2}{(2\bar{n}+1)^2U^2} \right) + \mathcal{O}\left(\frac{J^4}{U^3}\right). \quad (26)$$

In particular, one sees that v_{\max} is a decreasing function of U/J .

For the strictly positive quasiparticle energies (23), the ground state at a value of U and J is the quasiparticle vacuum

$$|\psi_0(U/J)\rangle = \prod_k v^{-1}(k) \gamma_{k,+} \gamma_{-k,-} |\bar{n}\rangle \quad (27a)$$

$$= \prod_k (u(k) + v(k) c_{k,+}^\dagger c_{-k,-}^\dagger) |\bar{n}\rangle. \quad (27b)$$

The ground state at infinitely strong interactions, i.e. the Fock state with \bar{n} particles per site, $|\bar{n}\rangle$, represents the vacuum of the bare excess particles and holes.

D. Local observables and correlation functions

We summarize in this Sec. some general properties of the correlation functions in the quasiparticle formalism that will be used later to derive ground state and non-equilibrium properties of the system.

For the ground state (27), but also for the time-dependent wave functions (48) which will be introduced in section V, the only non-vanishing single-particle correlation functions are

$$\begin{aligned} g_d^{\sigma,\sigma} &= \langle c_{j+d,\sigma}^\dagger c_{j,\sigma} \rangle \\ &= \frac{1}{2\pi} \int_{-\pi}^{\pi} dk e^{-ikd} \langle c_{k,\sigma}^\dagger c_{k,\sigma} \rangle, \end{aligned} \quad (28a)$$

$$\begin{aligned} g_d^{\sigma,\bar{\sigma}} &= \langle c_{j+d,\sigma} c_{j,\bar{\sigma}} \rangle = \langle c_{j,\sigma}^\dagger c_{j+d,\bar{\sigma}}^\dagger \rangle^* \\ &= \frac{1}{2\pi} \int_{-\pi}^{\pi} dk e^{-ikd} \langle c_{k,\sigma} c_{-k,\bar{\sigma}} \rangle, \end{aligned} \quad (28b)$$

where $\bar{\sigma} = -\sigma$ and the thermodynamic limit has been taken. Possible time dependence (equal time) is implicit and expectation values are site-independent for the homogeneous systems under consideration. We note that the correlations of the different types are equivalent:

$$g_d^{+,+} = g_d^{-,-}, \quad g_d^{+,-} = g_d^{-,+}. \quad (29)$$

Therefore, also the quasiparticle densities do not depend on the flavor and we can define a single density of excitations:

$$n_{\text{ex}} = \langle n_{j,+} \rangle + \langle n_{j,-} \rangle = 2g_0^{\sigma,\sigma}. \quad (30)$$

Since the Hamiltonian is quadratic, correlations of the occupancies can be related to the single-particle correlations using Wick's theorem, which gives us

$$G_d^{\sigma,\sigma'} = \langle n_{j+d,\sigma} n_{j,\sigma'} \rangle - \langle n_{j+d,\sigma} \rangle \langle n_{j,\sigma'} \rangle \quad (31)$$

$$= -\sigma\sigma' |g_d^{\sigma,\sigma'}|^2. \quad (32)$$

In the special case $d = 0$, the fermionic statistics, together with the symmetry with respect to exchange of fermionic flavor, imply that the on-site correlator $G_{d=0}^{\sigma,\bar{\sigma}} = |g_{d=0}^{\sigma,\bar{\sigma}}|^2$ vanishes and the local double occupancy factorizes:

$$\langle n_{j,\sigma} n_{j,\bar{\sigma}} \rangle = \langle n_{j,\sigma} \rangle \langle n_{j,\bar{\sigma}} \rangle = n_{\text{ex}}^2/4. \quad (33)$$

The density of excitations thus fully determines all local properties, including the atom number fluctuations:

$$f = \langle (n_j - \bar{n})^2 \rangle = n_{\text{ex}}(1 - n_{\text{ex}}/2). \quad (34)$$

Atom correlations can be related to correlations of auxiliary particles. Making use of Eq. (11), we can for example express atomic density correlations in the following way:

$$C_d = \langle n_j n_{j+d} \rangle - \langle n_j \rangle \langle n_{j+d} \rangle \quad (35)$$

$$= \sum_{\sigma} (G_d^{\sigma,\sigma} - G_d^{\sigma,\bar{\sigma}}) \quad (36)$$

$$= -2(|g_d^{+,+}|^2 + |g_d^{+,-}|^2). \quad (37)$$

Ultracold atom experiments with single-site resolved imaging [55, 56] can access the parity $s_j = e^{i\pi(n_j - \bar{n})}$ rather than the density itself. The expression for parity correlations turns out to be similar to that of density correlations:

$$S_d = \langle s_j s_{j+d} \rangle - \langle s_j \rangle \langle s_{j+d} \rangle \quad (38)$$

$$= 4 \sum_{\sigma} (G_d^{\sigma,\sigma} + G_d^{\sigma,\bar{\sigma}}). \quad (39)$$

Both density and parity correlations are particularly simple to evaluate within the present approach. Correlations including the non-local string operator (7), such as the single-particle correlations $\langle a_j^\dagger a_{j+d} \rangle$, can also be computed, but they require the evaluation of the Toeplitz determinant [57]. Interestingly, the fermionic string (7) is equivalent to the string operator recently measured by Endres *et al.*[58].

IV. EQUILIBRIUM PROPERTIES OF THE MOTT-INSULATING PHASE

In this section we discuss the equilibrium properties of the Mott-insulating phase derived within the unconstrained fermion approximation.

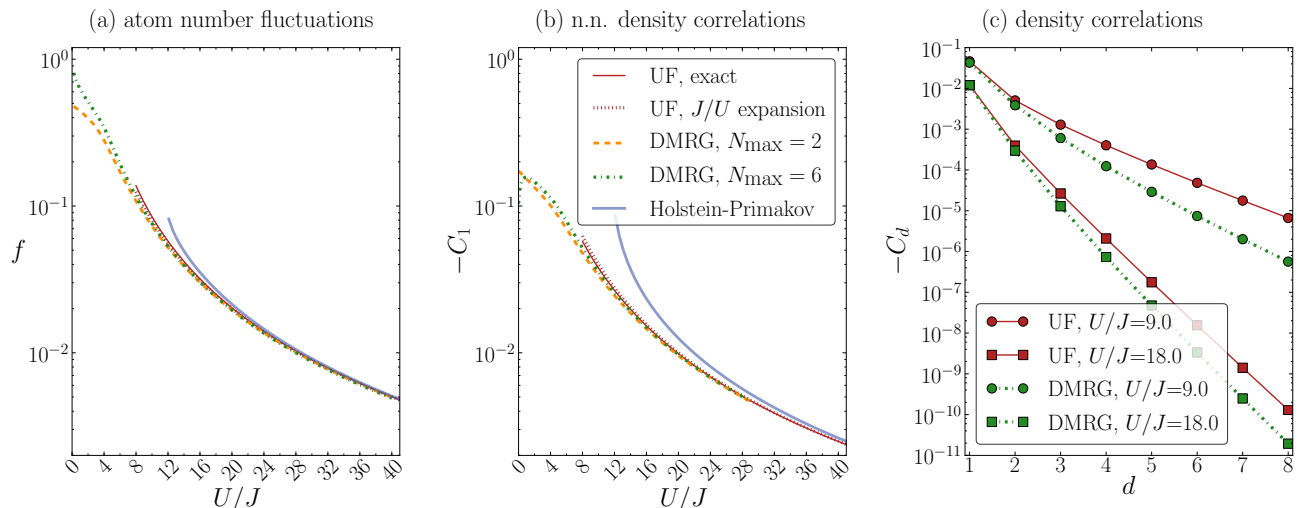


FIG. 2. (Color online) Ground state properties at $\bar{n} = 1$. The numerical evaluation of the UF equations is compared with the strong coupling expansion, as well as with exact DMRG simulations of the Bose–Hubbard model with the local Hilbert space truncated at a maximum site occupancy of either $N_{\max} = 2$ or $N_{\max} = 6$. (a) Atom number fluctuation f as a function of the final interaction strength U/J . (b) Nearest-neighbor density correlation $C_{d=1}$ as a function of the final interaction strength U/J . (c) Density correlations as a function of the distance d .

As argued in the preceding section, the observables are related to single-particle correlations (28), which for the ground state (27) can be evaluated straightforwardly:

$$\langle c_{k,\sigma}^\dagger c_{k',\sigma} \rangle = -\delta_{k,k'} v^2(k), \quad (40)$$

$$\langle c_{k,\sigma} c_{-k',\bar{\sigma}} \rangle = \delta_{k,k'} u(k)v(k), \quad (41)$$

with the coefficients $u(k)$ and $v(k)$ given in Eq. (19). The local density of excitations (30) can thus be calculated from

$$n_{\text{ex}} = -\frac{1}{\pi} \int_{-\pi}^{\pi} dk v^2(k). \quad (42)$$

In the case of strong interactions, one can also derive an explicit expression from the expansion (19b) and (19d) of the coefficients $u(k)$ and $v(k)$:

$$n_{\text{ex}} = \frac{2J^2}{U^2} \bar{n}(\bar{n} + 1) + \mathcal{O}\left(\frac{J^4}{U^4}\right). \quad (43)$$

Combining Eqs. (33) and (43) gives an estimate of the occupation of unphysical states (16),

$$p_{+-} = n_{\text{ex}}^2/4 \lesssim (8(1 + 1/\bar{n}))^{-2}, \quad (44)$$

where the right-hand side stems from the evaluation of (43) at the lowest interaction considered (23). For $\bar{n} = 1$, p_{+-} is less than 6% and we expect the error on local expectation values to be of similar magnitude. With this at hand, we can now consider the behavior of the density correlations in the ground state. In Fig. 2(a), the atom

number fluctuation $f = n_{\text{ex}}(1 - n_{\text{ex}}/2)$ is evaluated numerically using (42) and compared to the strong coupling expansion (see also [59])

$$f = \frac{2J^2}{U^2} \bar{n}(\bar{n} + 1) + \mathcal{O}\left(\frac{J^4}{U^4}\right), \quad (45)$$

as well as to the results obtained from DMRG simulations with a truncation of the site occupancy to $N_{\max} = 2$ or $N_{\max} = 6$ (system size is 256 sites, 400 DMRG-states are retained). The predictions of the UF approximation, both from the numerical integration of (42) and from the strong coupling expansion, are in excellent agreement with the DMRG simulations for all interaction strengths satisfying (23). The accuracy of the truncation of the local Hilbert space to three states only is also confirmed by the DMRG simulations. Higher occupancies start to be important only for interaction strengths below the point where the UF approximation breaks down.

We further compare our results with the ones derived within a Holstein–Primakov approximation of the slave-boson representation used, e.g., by Huber *et al.* [35]. This approach is equivalent to the auxiliary boson representation (2) when fully relaxing the constraints (4,5). We find that the local observables cannot be well described at intermediate interaction strengths, even though the density of excitations is small (Fig. 2). A similar instability has been observed with slave bosons in Ref. [47]. We will analyze the slave-boson approach in more detail later in the context of the non-equilibrium dynamics (Sec. V D).

We can also evaluate analytically non-local density cor-

relations to second order in J/U :

$$C_d = -\frac{J^2}{U^2} \bar{n}(\bar{n} + 1) \delta_{d,1} + \mathcal{O}\left(\frac{J^4}{U^4}\right). \quad (46)$$

As shown in Fig. 2(b), the above expression only slightly overestimates the amplitude of the correlations compared to the full numerical evaluation of the integrals (28) and (37) with (41). We therefore conclude that local observables and nearest-neighbor correlations in the Mott-insulator regime are well described by a perturbation expansion to order J^2/U^2 . This is no longer the case for longer-range correlations, which are simply vanishing according to the expansion to second order, whereas the exact DMRG predicts that they should be finite and exponentially decaying. As can be seen in Fig. 2(c), the numerical evaluation of the UF equations provides a much better agreement with the DMRG results. The correlations at $d = 2$ can be almost perfectly reproduced and a similar decay length is found. The amplitude of the correlations for $d > 2$ is overestimated, however, and the discrepancy becomes worse as d increases.

V. QUENCH DYNAMICS – GENERAL DESCRIPTION

We analyze the quench dynamics of a system prepared initially in a deep Mott-insulating state. We first derive the general results for the time evolution of the wave function and the correlation functions and then give explicit expressions for the case where the initial state is a Fock state (infinite interactions). These results form the basis for the detailed discussion of the physical properties of the quench dynamics in the subsequent Sec. VI.

A. Time-dependent wave function and correlations

The initial state considered is the ground state at some values of J and U satisfying the condition (23) and takes the form

$$|\psi_{\text{init}}\rangle = \prod_k \left(u_0(k) + v_0(k) c_{k,+}^\dagger c_{-k,-}^\dagger \right) |\bar{n}\rangle. \quad (47)$$

The time-evolution of this state under the Hamiltonian H_{UF} reads

$$\begin{aligned} |\psi(t)\rangle &= e^{-iH_{\text{UF}}t/\hbar} |\psi_{\text{init}}\rangle \\ &= \prod_k \left(\bar{u}(k) - \bar{v}(k) e^{-i2\omega(k)t} \gamma_{k,+}^\dagger \gamma_{-k,-}^\dagger \right) |\psi_0(U/J)\rangle, \end{aligned} \quad (48)$$

with

$$\bar{u}(k) = u(k)u_0(k) - v(k)v_0(k), \quad (49a)$$

$$\bar{v}(k) = v(k)u_0(k) - u(k)v_0(k). \quad (49b)$$

For the wave function (48), the non-vanishing equal-time single-particle correlations evaluate to

$$\begin{aligned} \langle c_{k,\sigma}(t) c_{-k',\bar{\sigma}}(t) \rangle &= \delta_{k,k'} u(k) \bar{u}(k) \left[e^{-2i\omega(k)t} u(k) \bar{v}(k) - \bar{u}(k) v(k) \right] \\ &\quad + \delta_{k,k'} v(k) \bar{v}(k) \left[e^{2i\omega(k)t} v(k) \bar{u}(k) - \bar{v}(k) u(k) \right] \end{aligned} \quad (50a)$$

and

$$\begin{aligned} \langle c_{k,\sigma}^\dagger(t) c_{k',\sigma}(t) \rangle &= \delta_{k,k'} [2 \cos(2\omega(k)t) u(k) \bar{u}(k) v(k) \bar{v}(k) \\ &\quad u^2(k) \bar{v}^2(k) - v^2(k) \bar{u}^2(k)]. \end{aligned} \quad (50b)$$

Based on these expressions, the expectation values of any observables be either calculated analytically, when the strong coupling expansion holds, or computed numerically for lower interactions (see III D).

B. Strong coupling expansion

For concreteness, we focus now on a quantum quench starting from the Fock state with filling \bar{n} by setting $u_0(k) = 1$, $v_0(k) = 0$ and thus $\bar{u}(k) = u(k)$, $\bar{v}(k) = v(k)$. In this case, the expansion in J/U leads to

$$\begin{aligned} \langle c_{k,\sigma}(t) c_{-k,\bar{\sigma}}(t) \rangle &= i \frac{2J\sqrt{\bar{n}(\bar{n}+1)}}{U} \sin(k) \left[e^{-2i\omega(k)t} - 1 \right] \\ &\quad + \mathcal{O}\left(\frac{J^2}{U^2}\right), \end{aligned} \quad (51a)$$

$$\begin{aligned} \langle c_{k,\sigma}^\dagger(t) c_{k,\sigma}(t) \rangle &= \frac{8J^2\bar{n}(\bar{n}+1)}{U^2} \sin^2(k) [\cos(2\omega(k)t) - 1] \\ &\quad + \mathcal{O}\left(\frac{J^4}{U^4}\right), \end{aligned} \quad (51b)$$

where $\omega(k)$ stands for the dispersion in the strong coupling expansion (22b).

Within this expansion, the dynamics of the local density of excitations can be expressed in terms of the Bessel functions of the first kind, $\mathcal{J}_n(z) = \frac{i^{-n}}{2\pi} \int_{-\pi}^{\pi} dk e^{-iz \cos(k) + nk}$. One gets

$$n_{\text{ex}}(t) \approx \frac{8\bar{n}(\bar{n}+1)J^2}{U^2} \left[1 - \cos(Ut/\hbar) \left(\mathcal{J}_2(\tilde{J}t) + \mathcal{J}_0(\tilde{J}t) \right) \right], \quad (52)$$

with $\tilde{J} = 2J(2\bar{n} + 1)/\hbar$. In the relevant interaction regime, the population of unphysical states $p_{+-}(t)$ thus remains as small as in the ground state (44) and we expect the UF approximation to be well behaved in general. It is, however, important to note, that the expansion is not rigorous since the approximate dispersion (22b) is multiplied by time, which is unbounded.

The single-particle correlators required to derive non-local density correlations (37) read

$$\begin{aligned} g_d^{\sigma,\bar{\sigma}}(t) &\approx i \frac{2J\sqrt{\bar{n}(\bar{n}+1)}}{2\pi U} \int dk e^{ikd} \sin(k) \left[e^{-2i\omega(k)t} - 1 \right] \\ &= (-i)^{d+1} \frac{\sqrt{\bar{n}(\bar{n}+1)}J}{U} \left[e^{iUt/\hbar} (\mathcal{J}_{d+1}(\tilde{J}t) \right. \\ &\quad \left. + \mathcal{J}_{d-1}(\tilde{J}t)) + \delta_{d,1} \right]. \end{aligned} \quad (53)$$

Making use of the identity

$$\mathcal{J}_{d+1}(z) + \mathcal{J}_{d-1}(z) = \frac{2d}{z} \mathcal{J}_d(z), \quad (54)$$

we obtain the following expressions for the non-local density correlations:

$$C_{d=1}(t) \approx - \left(\frac{2\bar{n}(\bar{n}+1)Jd}{U} \right)^2 \left(\frac{\mathcal{J}_d(\tilde{J}t)}{\tilde{J}t} 2 \cos(Ut/\hbar) + 1 \right), \quad (55a)$$

$$C_{d>1}(t) \approx - \left(\frac{\bar{n}(\bar{n}+1)Jd}{U} \right)^2 \left(\frac{\mathcal{J}_d(\tilde{J}t)}{\tilde{J}t} \right)^2. \quad (55b)$$

We note that the interaction strength U is involved only in the magnitude of the correlations for $d > 1$, via the dimensionless parameter J/U . In the case of nearest-neighbor correlations, we find an additional oscillation of the amplitude with frequency U/\hbar .

C. Accuracy of the UF approximation

In this section, we analyze the accuracy of the successive approximations that lead from the Bose–Hubbard model to the UF approximation and its strong coupling expansion. For this purpose, we introduce the root-mean-square differences

$$\chi_d^2 = \frac{\int_0^{t_{\max}} dt \left(C_d^{(2)}(t) - C_d^{(1)}(t) \right)^2}{\int_0^{t_{\max}} dt \left(C_d^{(2)}(t) \right)^2}, \quad (56)$$

where $C_d^{(1)}$ and $C_d^{(2)}$ are the density correlations predicted using two different level of approximations. By observing the dependency of χ_d^2 with the distance d , we can verify, in particular, whether a given approximation breaks down at large times. For non-averaged results we refer to Sec. VI. We use $t_{\max} = 3\hbar/J$, the maximal time accessible by our DMRG simulations. We use a DMRG algorithm in the thermodynamic limit [60, 61], with a second-order Suzuki–Trotter decomposition of time step $\Delta t = 0.02\hbar/U$, and we retain 2400 states. The numerical error is always smaller than the symbol size and line width.

In Fig. 3(a), we first compare the strong coupling expansion (55) and the numerical evaluation of the UF approximation. We find that the expansion is relatively accurate ($\chi_d^2 < 10^{-1}$) down to interactions $U/J \sim 10$, except for the $d = 2$ correlation, which only slowly converges to the exact results when U/J is increased. We recall here that a similar accuracy is reached for the ground state correlations (Fig. 2).

In Fig. 3(b), we then compare the numerical evaluation of the UF approximation with the exact DMRG simulation of the Hamiltonian (12), i.e. the Bose–Hubbard model when the site occupancy is truncated to $N_{\max} = 2$. The UF approximation appears to be accurate within $\chi_d^2 < 10^{-1}$ for $U/J \gtrsim 12$. As we will show in Sec. VIC, the UF approximation still qualitatively describes the dynamics between $U/J \approx 12$ and $U/J = 8$, which marks the break down of the quasiparticle picture.

Finally, we compare in Fig. 3(c) the predictions of the DMRG simulation when the local Hilbert space is truncated to a maximum site occupancy $N_{\max} = 2$, corresponding to the model (12), or $N_{\max} = 6$. We observe that the error due to the truncation starts to be significant ($\chi_d^2 > 10^{-1}$) only for $U/J < 6$, i.e. when the interaction energy becomes larger than the width of the quasiparticle band.

D. Comparison with the Holstein–Primakov approximation for auxiliary bosons

In order to generalize the description to higher dimensions, it may appear tempting to fully relax the hardcore constraint (4) and work with bosons instead of fermions. The resulting Hamiltonian is then equivalent to the one derived by Huber *et al.* [35] using Holstein–Primakov bosons (HP). The resulting equations for the quasiparticles and their dispersions are very similar to those derived in the fermionic model, except that the coefficient $v(k)$ becomes symmetric instead of antisymmetric. As a consequence, local pairing of different species is no longer suppressed and the occupation of the unphysical states becomes much larger than in the fermionic approach. In order to quantify this effect, one first has to calculate the single-particle correlations. To lowest order in J/U , the quasiparticle coefficient takes the form $v(k) \stackrel{\text{HP}}{\approx} \frac{2J\sqrt{\bar{n}(\bar{n}+1)}}{U} \cos(k)$ and one finds

$$g_d^{\sigma,\bar{\sigma}}(t) \stackrel{\text{HP}}{\approx} \frac{2J\sqrt{\bar{n}(\bar{n}+1)}}{2\pi U} \int dk e^{ikd} \cos(k) \left[e^{i\tilde{J} \cos(k)t} - 1 \right], \quad (57)$$

which can be compared to the fermionic version (53). In particular, one finds that the integral (57) has a finite value at $d = 0$ and the overcompleteness

$$p_{+-} \stackrel{\text{HP}}{\approx} \frac{2\bar{n}(\bar{n}+1)J^2}{U^2} \mathcal{J}_1(\tilde{J}t) \quad (58)$$

becomes of the same order as the density of excitations and the density correlations. This means that physical

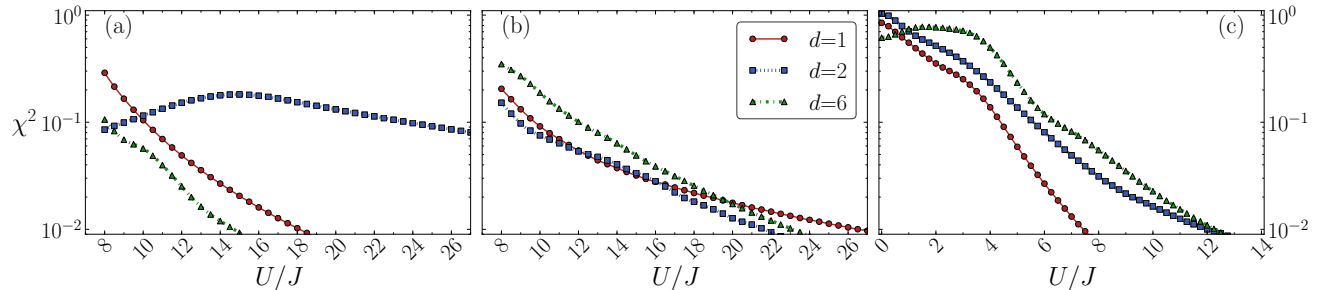


FIG. 3. (Color online) Root-mean-square differences χ^2 of the density correlations (56) obtained from different degrees of approximation. (a) The strong coupling expansion is compared to the numerical evaluation of the UF approximation. (b) The numerical evaluation of the UF approximation is compared to the exact DMRG simulation of the Bose–Hubbard model with a local site occupancy truncated at $N_{\max} = 2$. (c) The DMRG simulation with $N_{\max} = 2$ is compared to the DMRG simulation truncated at $N_{\max} = 6$.

and unphysical states play an equally important role in the HP approximation and this approach fails to describe the quench dynamics even in the limit $U \gg J$, where the density of excitations is low. This can be observed for example in the density correlations, which now read

$$C_{d>1}(t) \stackrel{\text{HP}}{\approx} - \left(\frac{\bar{n}(\bar{n}+1)J}{2U} \right)^2 \left[\mathcal{J}_{d-1}(\tilde{J}t) - \mathcal{J}_{d+1}(\tilde{J}t) \right]^2. \quad (59)$$

The change of sign between the two Bessel functions compared to the UF expressions has a dramatic effect, since the function in square brackets is now proportional to the derivative of a Bessel function, instead of a Bessel function itself (54). This leads in particular to the smearing out of one of the main features of the quench dynamics, namely the propagating correlation peak that we will describe in Sec. VI C.

E. Limit of non-interacting bosons

In this section, we complement the preceding analysis of quenches on the strongly interacting side by the extreme situation of a quench from infinite to zero interactions [33, 62]. At $U/J = 0$, the time evolution is readily described in the Heisenberg picture,

$$a_j(t) = \sum_{j'=1}^L V_{j,j'}(t) a_{j'},$$

in which individual bosons propagate with free dispersion. In the thermodynamic limit, this yields the propagator

$$\begin{aligned} V_{j,j+d}(t) &= \frac{1}{2\pi} \int_{-\pi}^{\pi} dk \exp[-i(2J \cos(k)t/\hbar - kd)] \\ &= (i)^d \mathcal{J}_d \left(\frac{2Jt}{\hbar} \right). \end{aligned} \quad (60)$$

Using the following relation for the initial Fock state:

$$\langle \bar{n} | a_p^\dagger a_q a_r^\dagger a_s | \bar{n} \rangle = \bar{n}^2 \delta_{p,q} \delta_{r,s} + \bar{n}(\bar{n}+1)(1 - \delta_{p,q}) \delta_{p,s} \delta_{q,r}.$$

we can derive explicit equations for the density correlations:

$$\begin{aligned} C_d(t) &= \bar{n}^2 \left(\sum_j \mathcal{J}_j^2(2Jt/\hbar) \right)^2 \\ &\quad + \bar{n}(\bar{n}+1) \left(\sum_j \mathcal{J}_{j+d}(2Jt/\hbar) \mathcal{J}_j(2Jt/\hbar) \right)^2 \\ &\quad - \bar{n}(\bar{n}+1) \sum_j \mathcal{J}_{j+d}^2(2Jt/\hbar) \mathcal{J}_j^2(2Jt/\hbar) - \bar{n}^2 \\ &= -\bar{n}(\bar{n}+1) \sum_j \mathcal{J}_{j+d}^2(2Jt/\hbar) \mathcal{J}_j^2(2Jt/\hbar). \end{aligned} \quad (61)$$

Here we have used the properties $\mathcal{J}_n(u \pm v) = \sum_{m=-\infty}^{\infty} \mathcal{J}_{n \mp m}(u) \mathcal{J}_m(v)$ and $\mathcal{J}_d(0) = 0$ for $d \neq 0$.

VI. HOW QUASIPARTICLE PAIRS CARRY DENSITY CORRELATIONS ACROSS THE SYSTEM

We now analyze in detail how correlations spread in the quench dynamics starting from the Fock state with \bar{n} atoms per site within the Bose–Hubbard Hamiltonian (1). The description in terms of fermionic quasiparticles for intermediate and strong interactions (48), as well as the non-interacting solution (61), provide a firm basis for the interpretation of the outcome of the DMRG simulations and of recent experimental results [19] and allow for their extrapolation at long times, where no analytical solution is available so far.

A. Quasiparticle pairs

For concreteness, we restrict our discussion in the following to the filling $\bar{n} = 1$, where the $+$ -quasiparticles (17a) correspond to doublons and $-$ -quasiparticles (17b) to holons. The relevant processes involved in the quench dynamics can be best understood in the expansion of the wave function (48) to lowest order in the auxiliary fermion operators:

$$|\psi(t)\rangle = |\bar{n}\rangle + i\frac{2\sqrt{2}J}{U} \sum_k \sin(k) c_{k,+}^\dagger c_{-k,-}^\dagger |\bar{n}\rangle \quad (62a)$$

$$- i\frac{2\sqrt{2}J}{U} \sum_k \sin(k) e^{i6J \cos(k)t/\hbar} c_{k,+}^\dagger c_{-k,-}^\dagger |\bar{n}\rangle. \quad (62b)$$

In this representation, the state decomposes into two parts: a time-independent part (62a) consisting of the Fock state and the symmetric superposition of bound nearest-neighbor doublon-holon pairs, and a time-dependent part (62b) describing the superposition of propagating doublon-holon pairs. The dynamics following the quench is driven by the propagating pairs, whereas the steady state is solely determined by the bound pairs, as the contribution of the propagating pairs phases out at long times. At lowest order in J/U , the steady state simply corresponds to the ground state at the final interaction strength. Higher order terms in the strong coupling expansion would describe the population in the excited states. At $t = 0$, the bound and propagating pairs interfere destructively and one recovers the initial Fock state $|\bar{n}\rangle$. Finally, we note that the wave function (62) is equivalent to the one obtained within a time-dependent perturbation theory in Appendix A and can be used to derive the perturbative results presented in Sec. VB.

The doublon and the holon forming a propagating pair are produced initially on neighboring sites by a single hopping event and then move in opposite directions. The two quasiparticles are entangled, since the pair is described by a superposition state:

$$\left(c_{k,+}^\dagger c_{-k,-}^\dagger - c_{-k,+}^\dagger c_{k,-}^\dagger \right) |\bar{n}\rangle.$$

This ensures a constant atomic density and leads to strong bipartite entanglement as the pairs are stretched across the system [11]. The momentum distribution of the quasiparticle pairs is sine shaped, from which follows that the quasiparticles propagate as a wave packet. The maximal weight of the momentum distribution is located at the wave vector $|k| = \pi/2$, where the dispersion relation (22b) is close to being linear, and is characterized by the maximal group velocity $v_{\max} = 6J/\hbar$. The wave-packet structure of the propagation can also be made explicit by turning the sum over the momenta in (62b)

into a sum over the lattice sites:

$$\begin{aligned} & \sum_k \sin(k) e^{i6J \cos(k)t/\hbar} c_{k,+}^\dagger c_{-k,-}^\dagger |\bar{n}\rangle \\ &= \sum_{j,d} \frac{(-i)^d \hbar d}{3Jt} \mathcal{J}_d(6Jt/\hbar) c_{j,+}^\dagger c_{j+d,-}^\dagger |\bar{n}\rangle. \end{aligned} \quad (63)$$

In the above expression, one immediately recognizes the propagation velocity $6J/\hbar$ in the argument of the Bessel functions. However, we expect a large dispersion of the wave packet due to the width of the momentum distribution. A detailed description of the propagation of the quasiparticle pairs is left for Sec. VIC.

The situation is somewhat different for weakly interacting bosons. In the non-interacting solution (61), the correlation functions result from the interference between free bosons propagating with a relative velocity $4J/\hbar$. Unlike the auxiliary particles in the strongly interacting case, the number of free bosons per site is not limited, which leads to some qualitative differences that we will discuss later.

B. Correlation signal in the density correlations

The equal-time density correlations $C_d(t)$ in the strongly interacting limit exhibit a very peculiar feature for $d \geq 2$, namely, the presence of a negative signal, a dip, propagating to larger distances at longer times. This can be seen, for example, in Fig. 4, where we display the time evolution of these correlations for $U/J = 18$, as predicted by the UF approximation and the DMRG simulation (which are in remarkable agreement). This characteristic signal is already present in the perturbative result and can be attributed to the propagating quasiparticle pairs, illustrating the interest of this picture.

The structure of the nearest-neighbor correlation is more complicated. In the long-time limit and within the strong coupling expansion, the nearest-neighbor correlation reaches the value corresponding to the ground state at the final interaction strength. At short time, it exhibits oscillations driven by the interaction strength U and corresponding to the interaction of a holon (doublon) of the bound pair (62a) with a doublon (holon) of a propagating pair (62b). In the first order of the strong coupling expansion (62), the bound pairs extend only over a distance $d = 1$ but in the full numerical integration they can spread over larger distances [cf. Fig. 2(c)], leading to additional oscillations for $d = 2$. These oscillations are clearly visible in numerical evaluations of the correlations within the UF approximation, as well as in the DMRG simulations (Fig. 4).

While the UF approximation is almost exact at short distances, it overestimates the weak oscillations with period \hbar/U at larger distances. We found that these stem from terms of order J^4/U^4 dominating the doublon-doublon and holon-holon correlations. These oscillations are also present in the DMRG simulations, but with a

much lower amplitude. Interestingly, these terms cancel in the parity correlations studied in [19], where the UF approximation is in even better agreement with the exact simulations.

For quenches to intermediate values of the interaction strength, the dynamics of density correlations exhibits essentially the same features as described above. This can be seen in Fig. 5, where the dynamics following a quench to $U/J = 9$ is depicted. In particular, the characteristic dip corresponding to the propagating quasiparticles is still present. We note that the propagation of this correlation signal is still remarkably well described by the UF approximation, even though this model is close to breaking down at this interaction strength. However, one sees that the strong coupling expansion significantly overestimates the amplitude of the correlations at $d = 1$ and that the amplitude of the unphysical oscillations in the numerical evaluation of the UF approximation increases.

In the weakly interacting regime, one could expect a different behavior since the relevant quasiparticles are of different nature. However, the main features that characterize the dynamics of density correlations at strong and intermediate interactions are remarkably preserved, as can be seen in Fig. 6. In particular, a propagating dip can be identified in all cases. The main difference between the non-interacting (61) and the strongly interacting (55) cases is the lower velocity and very slow decay of correlations at long times when $U = 0$. At $U/J = 2$, this long tail is already strongly suppressed at short distances, but is still visible at longer distances. For $U/J = 4$ (Fig. 6), one sees that the overall profile of the propagating correlation signal is already very similar to that in the more strongly interacting case (Figs. 4 and 5).

At low interaction strengths, one has to be careful when using the DMRG simulations since the truncation of the local Hilbert space to a finite number of states can introduce significant errors. By comparing DMRG simulations to the exact formula (61) obtained in the “worst” case $U/J = 0$, we found that a maximal site occupancy $N_{\max} = 6$ represents a fairly safe approximation, whose accuracy improves with the distance for the times considered (see Fig. 6).

To summarize the analysis conducted in this section, we observe that the dynamics of the density correlations is dominated by the propagation of a negative signal (dip). For strong interactions, this dip results from the propagation of the quasiparticle pairs described in Sec. VI. In the next section we will investigate in more detail the shape of that signal and characterize its propagation velocity quantitatively.

C. Analysis of the signal propagation

We can get a lot of insight into the propagation of the signal from the following approximation of the density correlations at large distances (we recall that the lattice

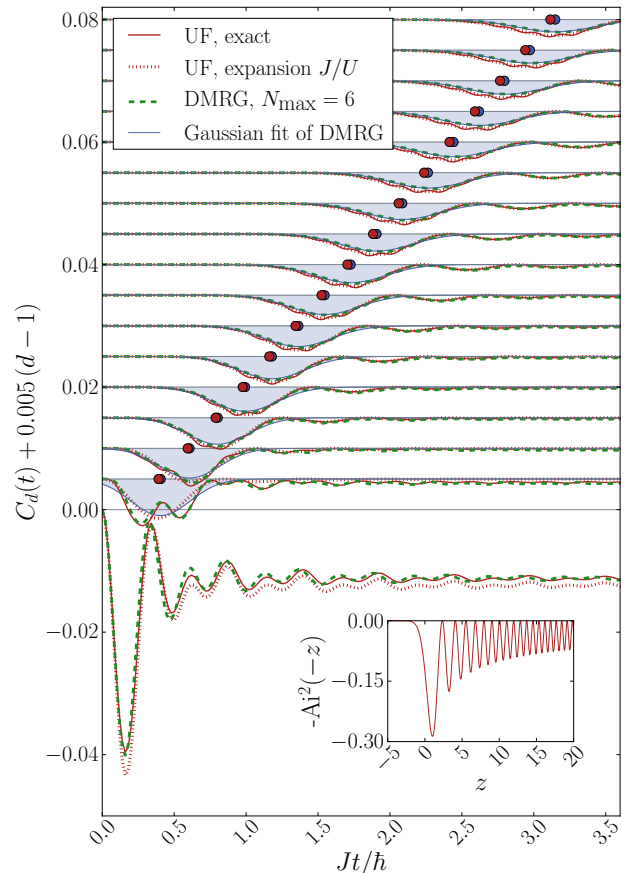


FIG. 4. (Color online) Dynamics of density correlations at distance $d \geq 1$ after a quench from the Fock state $|\bar{n}\rangle$ at infinite interactions to a final interaction $U/J = 18$. The results for different distances d are shifted for clarity by $0.005(d-1)$. We display the results obtained from the numerical evaluation of the UF equations, from their strong coupling expansion and from exact DMRG simulations. The shaded blue profiles figure a Gaussian fit of the correlation signal from the DMRG simulation, after the high-frequency oscillations have been filtered out. The filled blue circles mark the center of the fitted profile, i.e. the position of the signal. The filled red circles mark the position of the correlation signal obtained in the same way from the numerical evaluation of the UF approximation (fit not shown). The Airy function that appears in the analytical formulas derived from the UF approximation is plotted in the inset.

constant a_{lat} is set to one):

$$C_d \stackrel{d \gg 1}{\approx} - \left(\frac{2d^{2/3} 2^{1/3} \hbar}{3Ut} \right)^2 \text{Ai}^2 \left(-(2/d)^{1/3} (6Jt/\hbar - d) \right). \quad (64)$$

In the above expression, derived from (55b), we made use of the relation existing between the Airy function $\text{Ai}(-z)$ and the high-order Bessel functions [63]:

$$\mathcal{J}_d(d + zd^{1/3}) = 2^{1/3} d^{-1/3} \text{Ai}(-2^{1/3}z) + \mathcal{O}(d^{-1}). \quad (65)$$

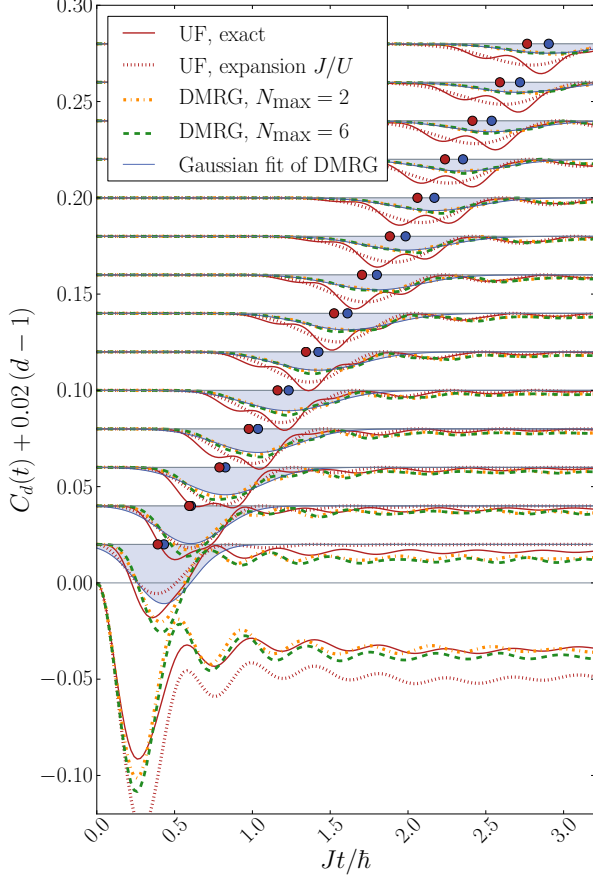


FIG. 5. (Color online) Dynamics of density correlations after a quench from the Fock state $|\bar{n}\rangle$ at infinite interactions to a final interaction $U/J = 9$. See Fig. 4 for more information.

The Airy function is plotted in the inset of Fig. 4. It exhibits a peak located at $z_0 \approx 1.02$ and surrounded by an exponential tail on the side $z < z_0$ and by an algebraically-decaying oscillating tail on the side $z > z_0$.

Disregarding the monotonically and slowly varying prefactor in Eq. (64), the profile of the Airy function alone allows us to understand several features of the propagation of the correlation signal. For example, it reveals the existence of a well defined propagation front, since the correlations are exponentially suppressed for times $t < t_{\text{peak}}$, with

$$\frac{Jt_{\text{peak}}}{\hbar} \approx \frac{1}{6} \left[d + z_0 \left(\frac{d}{2} \right)^{1/3} \right]. \quad (66)$$

The signal in the density correlations corresponds to the peak of the Airy function. Once this peak has passed, that is for $t > t_{\text{peak}}$, the correlations show an algebraic decay with oscillations. From the definition of t_{peak} , one sees that two terms contribute to the propagation of the correlation signal: the first is simply proportional

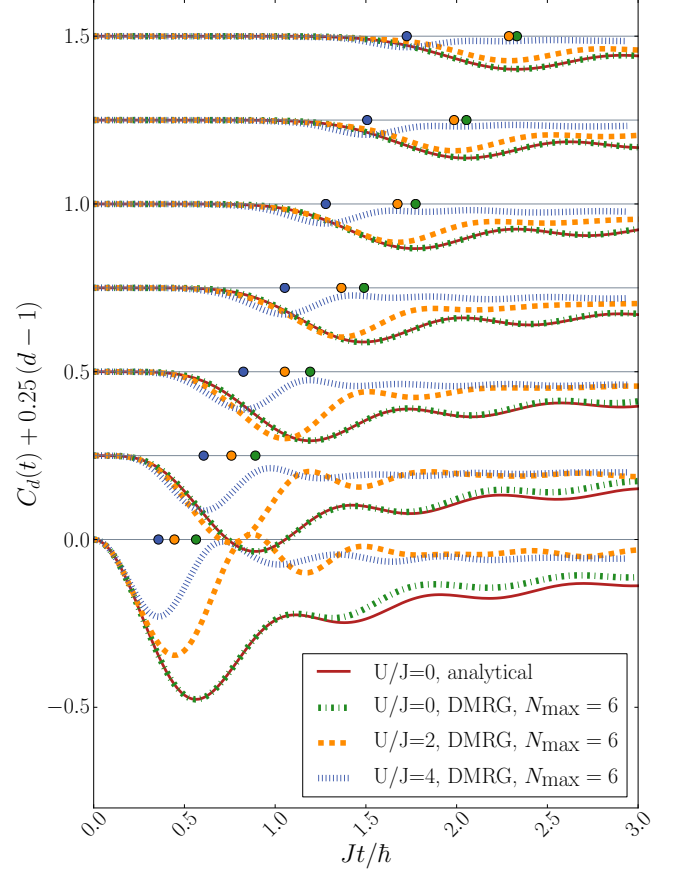


FIG. 6. (Color online) Dynamics of density correlations after a quench from a Fock state $|\bar{n}\rangle$ at infinite interactions to weak final interactions. The results for different distances d are shifted for clarity by $0.25(d-1)$. Unlike in Figs. 4 and 5, the position of the correlation signal of the DMRG results is identified with the position of the absolute minimum and it is denoted by the circles in the corresponding colors.

to the distance, corresponding to a well defined velocity, whereas the second is proportional to $d^{1/3}$. The linear contribution dominates at large distances, leading to a light-cone-like spreading of the correlations. At small distances, however, the dynamics deviates significantly from the asymptotic light cone. This behavior can be accounted for by defining an 'instantaneous' propagation velocity:

$$\begin{aligned} v_d &= [t_{\text{peak}}(d+1) - t_{\text{peak}}(d)]^{-1} \\ &= v_\infty \left(1 - \frac{z_0}{2^{1/3}3} d^{-2/3} \right) + \mathcal{O}(d^{-5/3}). \end{aligned} \quad (67)$$

One sees immediately in the above equation that the asymptotic light cone is characterized by the velocity $v_\infty = 6J/\hbar$ and is reached algebraically at large distances, whereas the propagation velocity can go down to approximately $4J/\hbar$ at short distances.

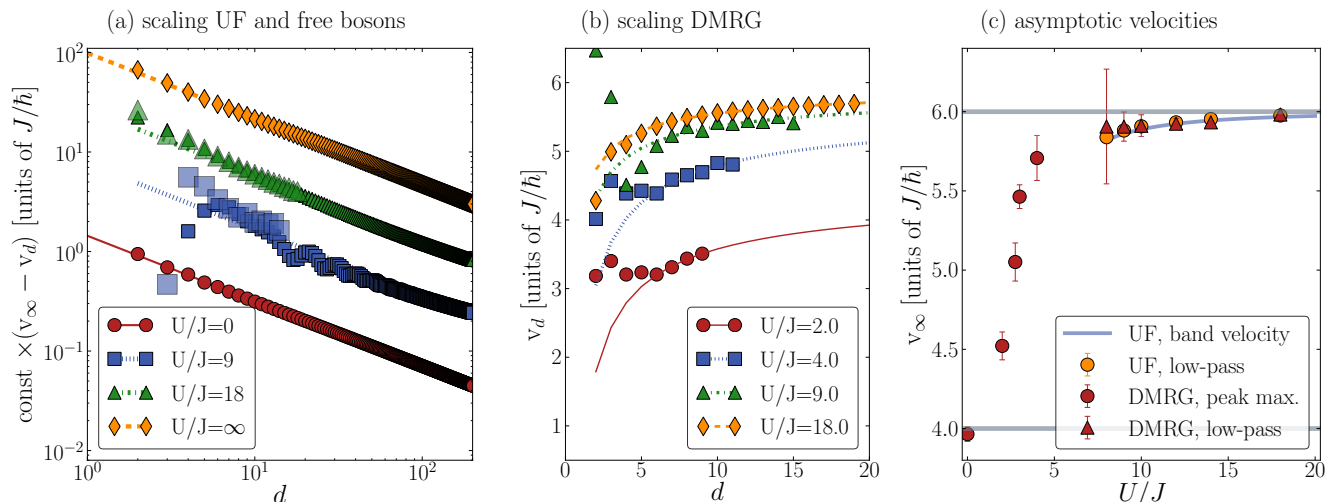


FIG. 7. (Color online) (a) Instantaneous propagation velocity in the UF approximation or in the non-interacting case as a function of the distance d (filled symbols). Light symbols represent DMRG data. Lines show the fits $|v_d - v_\infty| \propto d^{-\alpha}$. The data have been shifted vertically for a better visibility. (b) Instantaneous propagation velocity obtained by DMRG simulation as a function of the distance d (filled symbols). Lines show the fits $|v_d - v_\infty| \propto d^{-\alpha}$ with fixed exponent $\alpha = 0.65$. (c) Asymptotic velocities v_∞ extracted from the finite distance data versus interaction strength using $|v_d - v_\infty| \propto d^{-0.65}$. Error bars denote the 2-sigma uncertainty of the fit that yields the asymptotic velocity.

A similar analysis can be carried out for the case $U/J = 0$. It turns out that the correlation dip is almost completely described by a single term in the infinite sum (61). For even d , for example, we obtain:

$$\begin{aligned} C_d(t) &\approx -2J_{d/2}^4(2Jt/\hbar) \\ &= -2d^{-4/3}\text{Ai}^4\left(-d^{-1/3}(4Jt/\hbar - d)/2\right). \end{aligned} \quad (68)$$

The same expression for the instantaneous velocity (67) therefore holds in the non-interacting case as well, but with $v_\infty = 4J/\hbar$, which is the velocity of freely propagating bosons. The behavior at $U/J = 0$ mostly differs from the strongly interacting case once the correlation dip has passed ($t > t_{\text{peak}}$): further terms (61) beyond Eq. (68) then become important, which causes correlations to decay very slowly (see Fig. 6).

The width and the height of the correlation dip can also be derived from the expressions (64,68). For both the interacting and the non-interacting case, the width increases proportionally to $d^{1/3}$ while the height decreases with $d^{-2/3}J^2/U^2$ in the strongly interacting case and with $d^{-4/3}$ for $U/J = 0$. We note that similar power laws have been found for the quantum Ising model [23].

In the following, we show that the approximate scaling of the velocity found in the strongly and non-interacting limits holds for any interaction strength. We first concentrate on large interaction strengths. Within the UF approximation, we can evaluate the correlations up to arbitrarily long times and make a rigorous scaling analysis of the instantaneous propagation velocity. We determine the position of the dip by means of a Gaussian fit af-

ter having filtered out oscillations with a period shorter than h/U using a low-pass filter. Fig. 7(a) illustrates for a few interaction strengths that the analytical scaling behavior $|v_d - v_\infty| \propto d^{-\alpha}$ is accurately reproduced at sufficiently large distances $d > 5$. Extracting the asymptotic velocities v_∞ and the exponents α with a fit over distances $6 \leq d \leq 400$, we obtain values in very good agreement with the approximated analytical predictions. For example, the exponent is found to be the same for all interactions: $\alpha = 0.650 \pm 0.002$. The small difference from the value $\alpha = 2/3$ expected from the Airy functions (67) is most probably due to the prefactor in (64), which we neglected when deriving (67). The asymptotic velocities match the ones that we expect from the quasiparticle dispersion relation Eq. (25), as shown in Fig. 7(c). Close to the breakdown of the UF approximation, the oscillation frequencies due to the interaction and the finite bandwidth become similar and one cannot easily filter out the first one anymore. The instantaneous velocity v_d therefore shows an oscillatory behavior even at very large distances $d \lesssim 50$. Nevertheless, the scaling behavior remains perfectly obeyed on average and in the long-distance limit. In the non-interacting case, shown in Fig. 7(a), we extract accurately the position of the correlation signal by simply locating the first minimum. We again find the scaling exponent $\alpha = 0.650 \pm 0.002$ and the extracted asymptotic velocity is close to the expected value $v_\infty = 4J/\hbar$ [cf. Fig. 7(c)].

Using DMRG simulations, we can calculate the dynamics exactly for all interaction strengths, but we are restricted to short time and length scales. We therefore

fix the scaling exponent to $\alpha = 0.650$ in order to extract the asymptotic velocities. In Fig. 7(b) we show that the scaling $|v_d - v_\infty| \propto d^{-0.65}$ becomes accurate as the distance increases for both strong ($U/J \geq 8$, extracted with low-pass filter and Gaussian fit) and weak interactions ($U/J \leq 4$ extracted directly from the peak without low-pass filter). Despite the limited number of data points available in the scaling region, we can determine the asymptotic velocities with a reasonably small uncertainty. The values that we obtain, gathered in Fig. 7(c), are in good agreement with those predicted by the UF approximation. The lack of data in the range $4 < U/J < 8$ results from the mixing of the time scales related to kinetic and interaction processes and which prevents us from locating accurately the position of the correlation signal. The asymptotic velocities in Fig. 7(c) can be seen as a characterization of a crossover between a regime of quasi-free bosons ($U/J \lesssim 4$), with a renormalized velocity, and the strongly interacting regime described by two flavors of fermions. This crossover is not directly related to the ground-state phase diagram of the Bose-Hubbard model since the propagation velocity reflects the dispersion in the center of the Brillouin zone (at wave vectors $k \approx \pm \frac{\pi}{2}$), rather than low-wavelength modes. As a consequence, v_∞ is considerably higher than the sound velocity in the superfluid regime [64, 65] and a linear propagation with $v_\infty \lesssim 6J/\hbar$ is found at strong interactions, even though at equilibrium the system would be in the Mott-insulating phase.

As a final remark, we note that the dependency of the propagation velocity on U/J in that system has been studied before by Läuchli and Kollath [15], who considered the case of a quench from a small interaction strength to a larger one. Surprisingly, the instantaneous spreading velocity has been found to exhibit a maximum at intermediate interaction strength. A possible explanation for this effect could be that bosonic atom number fluctuations present in the initial superfluid state may lead to enhanced velocities as compared to the quench from the Fock state. A quantitative comparison between our predictions and this previous work would require an extrapolation of the velocity to large distances which is difficult in the absence of an analytical model.

VII. CONCLUSIONS

In order to describe accurately the quench dynamics of the one-dimensional Bose-Hubbard model in the Mott-insulating regime, we have developed a new analytical approach relying on the fermionization of auxiliary bosons. Its predictions regarding both the ground state and the dynamical properties are found in quantitative agreement with exact numerical simulations for large and intermediate interaction strengths $U/J > 8$. This constitutes a great improvement with respect to the analytical models introduced previously.

Using this model, we are able to investigate the time

evolution of density correlations in the quenched system over exceedingly long times. We observe a characteristic light cone dynamics, meaning that there exists a distance, linearly growing in time, beyond which correlations between distant sites are exponentially suppressed. More precisely, correlations spread as a wave packet along this light cone, forming a propagation front whose position can be unambiguously identified. A careful analysis of the velocity with which this front propagates reveals a generic scaling behavior characterized by a universal exponent and an asymptotic velocity dependent on the interaction strength. The same behavior is found in the non-interacting limit of freely propagating bosons, where an explicit solution is available, as well as in the intermediate regime $0 < U/J \leq 8$, where we rely on exact numerical simulations. The asymptotic velocity, which varies significantly between the weakly and the strongly interacting regime, is a useful quantity to characterize a broad spectral range of the Hamiltonian as it does not depend only on its low-lying modes.

Building upon this first success, we envisage that the representation of the Bose-Hubbard model in terms of fermionic quasiparticles could shed new light on the mechanism for thermalization or serve as a tool to interpret the outcome of spectroscopic measurement on laboratory systems, such as modulation spectroscopy or Bragg spectroscopy for ultracold gases in optical lattices.

ACKNOWLEDGMENTS

We thank D. Baeriswyl, T. Giamarchi, V. Gritsev, S. Huber and A. Tokuno for discussions. Financial support by ANR (FAMOUS), SNSF under Division II and MaNEP, and EU (Marie Curie Fellowship to M.C.) is acknowledged. P.B. thanks the University of Fribourg for hospitality.

Appendix A: Perturbation theory

In this appendix we develop a complementary perturbative approach to recover the behavior in the strong coupling limit to first non-vanishing order in J/U . The situation we consider is the quench from the Fock state $|\psi(0)\rangle = |\bar{n}\rangle$ at filling \bar{n} to a large final interaction strength U/J .

In all generality, the wave function after a sudden change of parameters can be written in the eigenbasis $|\phi_n\rangle$ (with corresponding eigenenergies E_n) of the final Hamiltonian

$$|\psi(t)\rangle = \sum_n e^{-it\frac{E_n}{\hbar}} \langle \phi_n | \psi(0) \rangle |\phi_n\rangle. \quad (\text{A1})$$

Usually the difficulty lies in determining the eigenstates $|\phi_n\rangle$ and their corresponding energies E_n in a many-body problem. In this appendix we determine $|\phi_n\rangle$ and E_n by perturbation theory in J/U in a system of length L with

periodic boundary conditions. Note, that this is not a full perturbative expansion, since we will not expand the exponential in the corresponding power.

We consider the interaction term of the Bose–Hubbard Hamiltonian as the unperturbed Hamiltonian and the kinetic part as the perturbation. The eigenenergies of the unperturbed Hamiltonian are multiples of the interaction strength U and the corresponding states are Fock states. More precisely, the ground state is the Fock state $|\bar{n}\rangle$ with vanishing energy. The lowest excited states are the states with a single particle-hole excitation with energy U . These we denote by $|\phi(m,d)\rangle$ with an occupation \bar{n} for all the sites except for site m with $\bar{n} + 1$ atoms and the site $m + d$ with $\bar{n} - 1$ atoms, i.e. $|\phi(m,d)\rangle = \frac{1}{\sqrt{\bar{n}(\bar{n}+1)}} b_{m+d} b_m^\dagger |\bar{n}\rangle$. Using degenerate perturbation theory (restricted to the same symmetry sector as the initial state) at first order in J/U , the ground state energy remains zero and the ground state of the final Hamiltonian is given by

$$|\phi_0\rangle \approx |\bar{n}\rangle + \frac{\sqrt{\bar{n}(\bar{n}+1)}J}{U} \sum_{m=0}^{L-1} (|\phi(m,1)\rangle + |\phi(m,-1)\rangle). \quad (\text{A2})$$

The lowest band of excited states resulting from the single particle-hole excitations is formed by

$$|\phi_p\rangle \approx |\phi_p^0\rangle - \frac{\sqrt{2\bar{n}(\bar{n}+1)}J}{U} \eta_p \sin(\pi p/L) |\bar{n}\rangle + J/U \sum_{\alpha} |\tilde{\phi}_{\alpha}\rangle \quad (\text{A3})$$

with corresponding energies

$$E_p \approx U - 2(2\bar{n} + 1)J \cos(\pi p/L). \quad (\text{A4})$$

Here $|\phi_p^0\rangle$ ($p = 0, \dots, L-1$) are the symmetric states that diagonalize the kinetic part of the Hamiltonian given by

$$|\phi_p^0\rangle = \frac{\sqrt{2}}{L} \sum_{d=1}^{L-1} \sum_{m=0}^{L-1} \sin(\pi p d/L) |\phi(m,d)\rangle.$$

Note that the index d only starts at 1 to avoid the double counting of the Fock state. We employed the notation $\eta_p = (1 - (-1)^p)$. As we are interested in the time-evolution of the initial Fock state, we abbreviated unimportant terms as $|\tilde{\phi}_{\alpha}\rangle$ which are the states beside the Fock state that are directly coupled via the kinetic term to the states $|\phi_p^0\rangle$.

Using these eigenenergies and states to first order, we can now write the time evolving state $|\psi(t)\rangle$ as

$$|\psi(t)\rangle = |\bar{n}\rangle + \frac{J\sqrt{\bar{n}(\bar{n}+1)}}{U} \sum_m (|\phi(m,1)\rangle + |\phi(m,-1)\rangle) - \frac{\sqrt{2\bar{n}(\bar{n}+1)}J}{U} \sum_p \eta_p \sin(\pi p/L) e^{-i\frac{E_p}{\hbar}t} |\phi_p^0\rangle. \quad (\text{A5})$$

This formula corresponds to the expression (62) which one obtains in the unconstrained fermionic approach up to first order. As discussed in the unconstrained fermionic approach this expression gives a lot of insight into the formation and propagation of singly and doubly occupied sites and can be used to compute all the observables that we are interested in.

-
- [1] S. Bravyi, M. B. Hastings, and F. Verstraete, Phys. Rev. Lett. **97**, 050401 (2006).
- [2] E. H. Lieb and D. W. Robinson, Commun. Math. Phys. **28**, 251 (1972).
- [3] J. Eisert, M. Cramer, and M. B. Plenio, Rev. Mod. Phys. **82**, 277 (2010).
- [4] M. B. Hastings, J. Math. Phys. **50**, 095207 (2009).
- [5] U. Schollwöck, Ann. Phys. **326**, 96 (2011).
- [6] T. Enss and J. Sirker, N. J. Phys. **14**, 023008 (2012).
- [7] B. Nachtergaele and R. Sims, Commun. Math. Phys. **265**, 119 (2006).
- [8] M. B. Hastings and T. Koma, Commun. Math. Phys. **265**, 781 (2006).
- [9] B. Nachtergaele and R. Sims, in *Entropy and the Quantum*, Contemporary Mathematics, Vol. 529, edited by R. Sims and D. Ueltschi (American Mathematical Society, 2010) pp. 141–176.
- [10] B. Nachtergaele and R. Sims, arXiv:1102.0835.
- [11] P. Calabrese and J. Cardy, Phys. Rev. Lett. **96**, 136801 (2006).
- [12] P. Calabrese and J. Cardy, J. Stat. Mech.: Theor. Exp. **2007**, P06008 (2007).
- [13] M. Cramer, A. Flesch, I. P. McCulloch, U. Schollwöck, and J. Eisert, Phys. Rev. Lett. **101**, 063001 (2008).
- [14] B. Nachtergaele, H. Raz, B. Schlein, and R. Sims, Commun. Math. Phys. **286**, 1073 (2008).
- [15] A. M. Läuchli and C. Kollath, J. Stat. Mech.: Theor. Exp. **2008**, P05018 (2008).
- [16] S.R. Manmana, S. Wessel, R. M. Noack, and A. Muramatsu, Phys. Rev. B **79**, 155104 (2009).
- [17] J. Eisert and D. Gross, Phys. Rev. Lett. **102**, 240501 (2009).
- [18] I. Bloch, J. Dalibard, and W. Zwerger, Rev. Mod. Phys. **80**, 885 (2008).
- [19] M. Cheneau, P. Barmettler, D. Poletti, M. Endres, P. Schauß, T. Fukuhara, C. Gross, I. Bloch, C. Kollath, and S. Kuhr, Nature (London) **481**, 484 (2012).
- [20] M. A. Cazalilla, Phys. Rev. Lett. **97**, 156403 (2006).
- [21] A. Iucci and M. A. Cazalilla, Phys. Rev. A **80**, 063619 (2009).
- [22] S. Sotiriadis and J. Cardy, Phys. Rev. B **81**, 134305 (2010).
- [23] F. Iglói and H. Rieger, Phys. Rev. Lett. **85**, 3233 (2000).
- [24] T. S. Cubitt and J. I. Cirac, Phys. Rev. Lett. **100**, 180406 (2008).
- [25] L. Mathey and A. Polkovnikov, Phys. Rev. A **81**, 033605

- (2010).
- [26] F. Goth and F. F. Assaad, arXiv:1108.2703v1.
- [27] L. Amico, A. Osterloh, F. Plastina, R. Fazio, and G. M. Palma, Phys. Rev. A **69**, 022304 (2004).
- [28] M. Rigol, A. Muramatsu, and M. Olshanii, Phys. Rev. A **74**, 053616 (2006).
- [29] G. De Chiara, S. Montangero, P. Calabrese, and R. Fazio, J. Stat. Mech.: Theor. Exp. , P03001 (2006).
- [30] P. Barmettler, A. M. Rey, E. Demler, M. D. Lukin, I. Bloch, and V. Gritsev, Phys. Rev. A **78**, 012330 (2008).
- [31] P. Barmettler, M. Punk, V. Gritsev, E. Demler, and E. Altman, New J. Phys. **12**, 055017 (2010).
- [32] H. Rieger and F. Iglói, Phys. Rev. B **84**, 165117 (2011).
- [33] S. S. Natu and E. J. Mueller, arXiv:1201.6674.
- [34] E. Altman and A. Auerbach, Phys. Rev. Lett. **89**, 250404 (2002).
- [35] S. D. Huber, E. Altman, H.P. Büchler, and G. Blatter, Phys. Rev. B **75**, 085106 (2007).
- [36] V. A. Kashurnikov and B. V. Svistunov, Phys. Rev. B **53**, 11776 (1996).
- [37] T. D. Kühner and H. Monien, Phys. Rev. B **58**, R14741 (1998).
- [38] A. R. Kolovsky and A. Buchleitner, Eur. Phys. Lett. **68**, 632 (2004).
- [39] C. Kollath, G. Roux, G. Biroli, and A. M. Läuchli, J. Stat. Mech.: Theor. Exp. , P08011 (2010).
- [40] S. R. White, Phys. Rev. Lett. **69**, 2863 (1992).
- [41] U. Schollwöck, Rev. Mod. Phys. **77**, 259 (2005).
- [42] G. Vidal, Phys. Rev. Lett. **91**, 147902 (2003).
- [43] A. J. Daley, C. Kollath, U. Schollwöck, and G. Vidal, J. Stat. Mech. , P04005 (2004).
- [44] S. R. White and A. E. Feiguin, Phys. Rev. Lett. **93**, 076401 (2004).
- [45] A. Auerbach, *Interacting Electrons and Quantum Magnetism* (Springer-Verlag, New York, 1994).
- [46] D. B. M. Dickerscheid, D. van Oosten, P. J. H. Denteneer, and H. T. C. Stoof, Phys. Rev. A **68**, 043623 (2003).
- [47] X. Lu, J. Li, and Y. Yu, Phys. Rev. A **73**, 043607 (2006).
- [48] A. Tokuno, E. Demler, and T. Giamarchi, arXiv:1106.1333.
- [49] P. Jordan and E. Wigner, Z. Phys. **47**, 631 (1928).
- [50] C. D. Batista and G. Ortiz, Phys. Rev. Lett. **86**, 1082 (2001).
- [51] M. Gutzwiller, Phys. Rev. Lett. **10**, 159 (1963).
- [52] T. Ogawa, K. Kanda, and T. Matsubara, Prog. Theor. Phys. **53**, 614 (1975).
- [53] M. Schiró and M. Fabrizio, Phys. Rev. B **83**, 165105 (2011).
- [54] S. D. Huber and G. Blatter, Phys. Rev. B **79**, 174504 (2009).
- [55] W. S. Bakr, J. I. Gillen, A. Peng, S. Fölling, and M. Greiner, Nature (London) **462**, 74 (2009).
- [56] J. F. Sherson, C. Weitenberg, M. Endres, M. Cheneau, I. Bloch, and S. Kuhr, Nature (London) **467**, 68 (2010).
- [57] E. Barouch and B. McCoy, Phys. Rev. A **3**, 786 (1971).
- [58] M. Endres, M. Cheneau, T. Fukuhara, C. Weitenberg, P. Schauss, C. Gross, L. Mazza, M. C. Banuls, L. Pollet, I. Bloch, and S. Kuhr, Science **334**, 200 (2011).
- [59] J. K. Freericks and H. Monien, Eur. Phys. Lett. **26**, 545 (1994).
- [60] G. Vidal, Phys. Rev. Lett **98**, 070201 (2007).
- [61] I. P. McCulloch, arXiv:0804.2509.
- [62] A. Flesch, M. Cramer, I. P. McCulloch, U. Schollwöck, and J. Eisert, Phys. Rev. A **78**, 033608 (2008).
- [63] M. Abramowitz and I. Stegun (Dover, 1964) Chap. 9.3.4.
- [64] E. H. Lieb, Phys. Rev. **130**, 1616 (1963).
- [65] C. Kollath, U. Schollwöck, J. von Delft, and W. Zwerger, Phys. Rev. A **71**, 053606 (2005).